UNIVERSITÀ DEL PIEMONTE ORIENTALE

SCHOOL OF MEDICINE
DEPARTMENT OF HEALTH SCIENCE

Master's degree in medical biotechnology

Graduation Thesis

Effects of blood-derived extracellular vesicles on proliferation and wound healing capacity of primary human dermal fibroblasts

Supervisor
Prof. Donato Colangelo

Firmato digitalmente da Donato Colangelo
Data: 29.06.2026 16:22:12 CEST
Organizzazione: UNIVERSITA' DEGLI STUDI DEL PIEMONTE ORIENTALE/01943490027

Co-supervisor
Dr. Stelvio Tonello

Candidate
Arianna Tugnolo
Matricola 20038123

Academic year 2025/2026

SUMMARY

Candidato
Arianna TUGNOLO
Matricola 20038123

Relatore
Prof. Donato Colangelo

Correlatore
Dott. Stelvio Tonello

Master's degree in medical biotechnology
Graduation Thesis

Effects of blood-derived extracellular vesicles on proliferation and wound healing capacity of primary human dermal fibroblasts

ABSTRACT

Rationale of the study: Extracellular vesicles (EVs) are nanosized particles released by virtually all cell types that carry a heterogeneous cargo of bioactive molecules and act as mediators of intercellular communication. Blood-derived EVs have attracted growing interest in the context of tissue repair, as they may modulate the behavior of cells involved in wound healing. Dermal fibroblasts play a central role in this process, contributing to extracellular matrix deposition, tissue remodeling and wound closure. This study aimed to evaluate whether blood-derived EVs can influence these repair-related functions in primary human dermal fibroblasts.
Planning of the study: EVs were isolated from peripheral blood of a healthy donor by ultracentrifugation and characterized in terms of size distribution and surface marker profile by nanoparticle tracking analysis (NTA) and MACSPlex flow cytometry. Effects of EVs on primary human dermal fibroblasts were evaluated by proliferation assay and wound healing assay, both performed with the Incucyte® system. Gene expression analysis by qRT-PCR was additionally performed following EV treatment.
Results: NTA and MACSPlex analysis confirmed the successful isolation of a heterogeneous EV population, enriched in platelet-derived vesicles as suggested by the high expression of CD42a and CD62P. In the proliferation assay, EV treatment influenced fibroblast confluency over time, with effects varying according to EV dilution and culture condition. In the wound healing assay, EV-treated fibroblasts showed increased wound closure compared with the respective controls. Gene expression analysis of CDKN1A did not reveal statistically significant differences between EV-treated cells and controls.
Conclusions: In conclusion, the data taken as a whole, support the hypothesis that EVs can have effects on some cell types. We have shown that characterized human blood derived EVs can play a relevant role in regenerative ability of primary human fibroblasts in different conditions and in absence of important physiological stimuli like serum. This study is preliminary and is limited by the number of experimental conditions. More data is necessary to understand if the proliferative capacity is linked to direct modulation of cell biochemistry or gene expression, and if gender, age and pathological conditions might affect this property.

1. INTRODUCTION

1.1 EXTRACELLULAR VESICLES (EVs)

Extracellular vesicles (EVs) are phospholipid bilayer-enclosed particles released into the extracellular environment that lack autonomous self-replicating ability[1]. These nanoscale vesicles are released by virtually all cell types as part of normal cellular activity and can be detected in a wide range of biological fluids, including blood, urine, saliva, and milk[2,3].

EVs carry a highly heterogeneous cargo composed of proteins, nucleic acids, lipids, and metabolites, which can be transferred to recipient cells, thereby modulating their biological behavior and mediating intercellular communication[2,4].

Initially regarded as simple cellular debris or waste disposal products, EVs are now recognized as key regulators of numerous physiological and pathological processes. Their intrinsic biocompatibility, low immunogenicity, ability to cross biological barriers, and capacity to mediate long-distance cellular communication have attracted increasing attention in biomedical research[3]. Over the past two decades, the EV field has expanded rapidly, highlighting their potential not only as non-invasive biomarkers for disease diagnosis and prognosis, but also as promising platforms for targeted therapeutic delivery[1,3].

1.1.1 CLASSIFICATION OF EVs

The classification of EVs has evolved significantly, moving from a simple tripartite model to a more complex landscape that accounts for diverse biogenesis pathways and physical properties. Traditionally, EVs are categorized into three main subtypes: exosomes, microvesicles (also called microparticles), and apoptotic bodies[5,6]. Exosomes are the smallest subtype (typically 30–150 nm) and originate from the endosomal system, specifically through the inward budding of late endosomes to form intraluminal vesicles (ILVs) within multivesicular bodies (MVBs), which are subsequently released upon fusion with the plasma membrane[5,6]. They are commonly characterized by biomarkers such as the tetraspanins CD9, CD63 and CD81 as well as ESCRT-related proteins like ALIX and TSG101[5]. In contrast, microvesicles range from 100 nm to 1,000 nm and are generated through the direct outward shedding or "budding" of the cell's plasma membrane, a process often triggered by cellular stress or activation signals[5,7]. Finally, apoptotic bodies represent the largest class with dimensions

ranging from 1 to 5 µm. They are uniquely produced during programmed cell death, frequently containing cellular debris, histones, and DNA[5,7].

Beyond these primary categories, recent research has identified specialized EV subpopulations based on their origin or pathological state, such as oncosomes (cancer-derived vesicles carrying oncogenic cargo), migrasomes (formed during cell migration), exomeres, supermeres, and membrane particles[6]. A significant challenge remains in the field due to the physical overlap in size and density between these subtypes, making complete separation difficult with current isolation techniques. Consequently, the International Society for Extracellular Vesicles (ISEV) recommends that researchers define EVs based on their physical and biochemical characteristics, such as size and surface protein composition, rather than relying solely on generic biogenetic terms[5].

1.1.2 BIOGENESIS OF EVs

The biogenesis of EVs involves distinct cellular pathways that define their molecular composition and biological function. Exosomes are generated through the endocytic pathway, beginning with the inward budding of the early endosomal membrane to form intraluminal vesicles (ILVs) within multivesicular bodies (MVBs)[5]. This process is mainly orchestrated by the endosomal sorting complex required for transport (ESCRT) machinery, where subunits like ESCRT-0 recognize ubiquitinated cargo and ESCRT-III mediate the final scission of the vesicle[5,8]. Alternatively, ESCRT-independent mechanisms utilize specialized lipids like ceramide, which possess a cone-shaped structure that spontaneously induces the membrane curvature required for ILV formation[9]. Microvesicles, instead, are formed by the direct outward "budding" and shedding of the plasma membrane into the extracellular space[8]. This outward fission requires the redistribution of membrane phospholipids, such as the movement of phosphatidylserine to the outer leaflet, and is driven by molecular cascades involving ADP-ribosylation factor 6 (ARF6) and the activation of myosin light chain kinase (MLCK)[5,9]. Overall, these different biogenetic mechanisms contribute to the heterogeneity of EV populations and influence their cargo composition and biological activity.

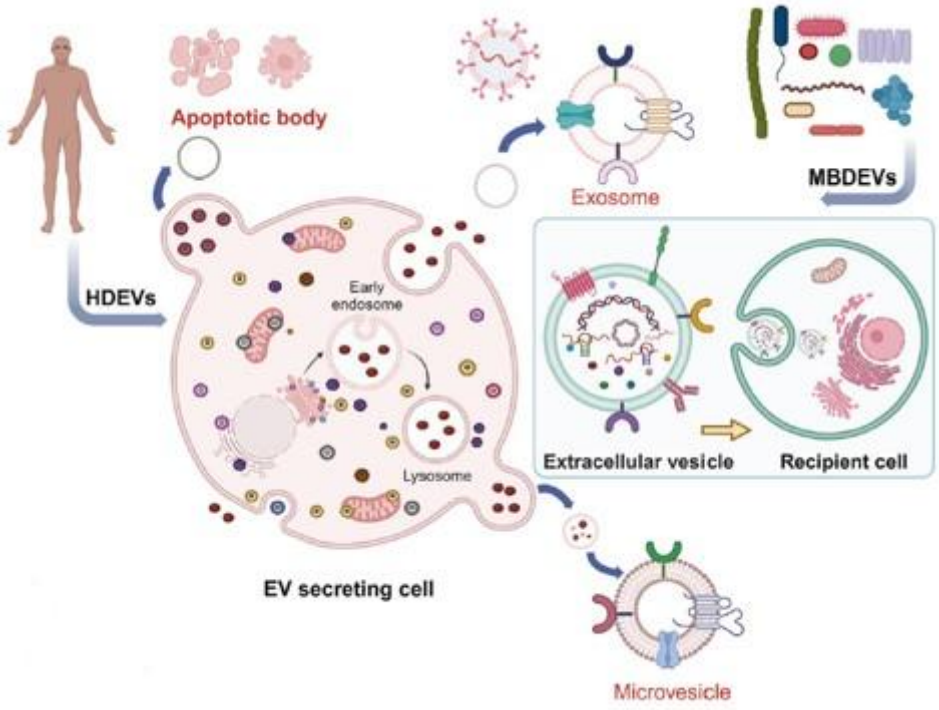

Figure 1 *- Schematic representation of extracellular vesicle biogenesis, sources and interaction with recipient cells. Extracellular vesicles (EVs) include human-derived EVs (HDEVs) and microbiota-derived EVs (MBDEVs), depending on their biological origin. EVs can be released through different biogenesis pathways and include subtypes such as exosomes, microvesicles and apoptotic bodies. Once released, EVs can transport bioactive cargo and interact with recipient cells, contributing to intercellular communication (modified from Kumar, M.A 2024)* [6].

1.1.3 CARGO AND BIOLOGICAL FUNCTION OF EVs

The molecular content of extracellular vesicles, commonly referred to as cargo, plays a central role in determining the biological activity of EVs. Cargo can be highly heterogeneous and reflects the cell of origin, its physiological or pathological state, and the surrounding microenvironment[10]. EVs can transport a broad range of bioactive molecules, including membrane and cytosolic proteins, tetraspanins, enzymes, lipids, metabolites, mRNA, miRNA, other non-coding RNAs and, in some cases, DNA[10,11]. Their lipid bilayer is essential for preserving this cargo in the extracellular environment, protecting it from enzymatic degradation and allowing the transfer of biological information to nearby or distant recipient cells[12].

Once released, EVs can interact with target cells through different mechanisms. They may activate signaling pathways through receptor–ligand interactions at the cell surface or deliver their cargo after membrane fusion or internalization through endocytic routes[11]. In this way, EVs contribute to intercellular communication and can influence several biological processes, including immune regulation, inflammation, angiogenesis, cell proliferation, migration,

differentiation, and tissue homeostasis[13]. These effects are highly context-dependent, as they vary according to EV source, cargo composition, and recipient cell type[10]. In tissue repair, this is particularly relevant because EVs may modulate the behavior of stromal cells, including fibroblasts, which are involved in extracellular matrix deposition, remodeling, and wound closure. For these reasons, EVs are increasingly investigated as both natural mediators of cellular communication and potential tools for regenerative medicine[14].

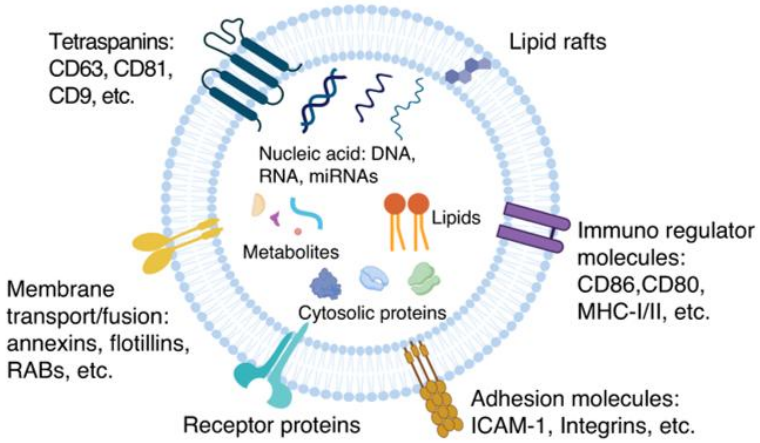

Figure 2 *- Schematic representation of the molecular cargo and surface components of extracellular vesicles. EVs contain different classes of bioactive molecules, including proteins, lipids, metabolites and nucleic acids, and display membrane-associated proteins involved in adhesion, signaling, immune regulation and vesicle transport [14].*

1.1.4 BLOOD-DERIVED EVs

Blood represents one of the most studied and complex sources for the analysis of extracellular vesicles, acting as a dynamic reservoir that can reflect the physiopathological state of the whole organism[15]. In this fluid, EVs form a highly heterogeneous mixture mainly originating from erythrocytes, leukocytes and platelets, together with rarer populations released by solid organs or tumor tissues[16]. Among them, platelet-derived EVs (pEVs) are considered the most abundant, accounting for approximately 30% of the total circulating EV pool[15].

These vesicles can retain surface molecules that reflect the identity and activation state of their parental cells[11]. For instance, markers such as CD42a, part of the GPIb-IX complex, and CD62P, also known as P-selectin, are commonly associated with platelet origin and platelet activation. In addition, the presence of integrins such as CD49e, also known as ITGA5, may contribute to cell adhesion and interactions with the extracellular matrix[15,17]. Due to their cargo, which can include growth factors such as PDGF, TGF-β and VEGF, as well as specific miRNAs, blood-derived EVs play an important role in intercellular communication and tissue

regeneration[15,17]. They may contribute to inflammatory responses and reparative processes by modulating the phenotype and activity of target cells[15]. In this context, their interaction with fibroblasts is especially relevant, as it may support cellular functions involved in tissue repair and wound healing.

1.2 FIBROBLASTS AND THEIR ROLE IN TISSUE REPAIR

Fibroblasts are mesenchymal stromal cells widely distributed throughout connective tissues and are primarily responsible for the synthesis, organization, and remodeling of the extracellular matrix (ECM)[18]. Beyond their structural role, fibroblasts actively contribute to tissue homeostasis by generating specialized microenvironmental niches and secreting cytokines, growth factors, metabolites, and other signaling molecules that regulate the behavior of neighboring cells[19].

Historically, fibroblasts were identified based on their characteristic spindle-shaped morphology within connective tissues; however, recent advances in single-cell technologies have revealed that they represent a highly heterogeneous and functionally diverse cell population. Distinct fibroblast subpopulations have been identified across different organs and even within the same tissue, where they exhibit specialized functions depending on their anatomical location and microenvironmental context[19,20].

Under physiological conditions, fibroblasts generally remain in a relatively quiescent state while continuously maintaining ECM turnover and tissue architecture[21]. Following tissue damage or disruption of homeostasis, they rapidly become activated and acquire enhanced proliferative, migratory, and matrix-remodeling capacities[22]. This remarkable plasticity allows fibroblasts to adapt their phenotype and function according to local tissue requirements, making them central regulators of tissue repair processes.

In the skin, dermal fibroblasts represent the major stromal cell population of the dermis and are essential for maintaining dermal structure and ECM composition. These cells are highly responsive to biochemical and mechanical cues from the surrounding matrix, which directly influence their survival, proliferation, migration, and functional activity[23]. For this reason, dermal fibroblasts are widely used as in vitro models to investigate cellular responses associated with tissue repair, including changes in proliferation and migratory behavior. Their

use is therefore particularly suitable for evaluating how bioactive stimuli may influence repair-related cellular functions[24].

1.3 WOUND HEALING PROCESS

Wound healing is a complex and highly coordinated biological process that aims to restore tissue integrity after injury and to re-establish the protective barrier function of the skin[25]. In humans, wound repair requires the temporal and spatial integration of several cellular and molecular events, including hemostatic responses, immune defense, cell migration, proliferation, ECM deposition, angiogenesis and tissue remodeling[26]. Although the process is often described as a linear sequence, wound healing occurs through overlapping and interdependent phases, classically divided into hemostasis, inflammation, proliferation and remodeling or maturation[27]. The duration and quality of each phase can vary according to the type and extent of injury, the local tissue microenvironment and systemic factors such as age, diabetes, vascular disease or other comorbidities[26].

Hemostasis represents the earliest response to tissue damage and has the immediate purpose of limiting blood loss and sealing the wound site[26]. Following vascular injury, blood vessels undergo vasoconstriction, while exposed collagen and ECM components promote platelet adhesion, platelet aggregation and activation of the coagulation cascade. This leads to the conversion of fibrinogen into fibrin and to the formation of a fibrin-rich clot, which acts not only as a physical barrier against fluid loss and pathogen entry, but also as a provisional scaffold for the migration of cells involved in later phases of repair[28]. Activated platelets also release growth factors and cytokines, including PDGF, TGF-β and VEGF, which contribute to the recruitment and activation of inflammatory cells, fibroblasts and endothelial cells[29].

The inflammatory phase begins shortly after injury and is essential for controlling infection, removing tissue debris and preparing the wound environment for tissue reconstruction[26]. Neutrophils are among the first immune cells recruited to the wound site, where they contribute to antimicrobial defense through phagocytosis, proteases, antimicrobial peptides and reactive oxygen species[30]. Monocytes are subsequently recruited and differentiate into macrophages, which remove cellular debris, produce cytokines and growth factors, and regulate the transition from inflammation toward tissue repair[29]. During this phase, macrophages undergo dynamic phenotypic changes, moving from a mainly pro-inflammatory

profile toward pro-resolving functions that help terminate inflammatory signaling and support later reparative events[26]. A balanced inflammatory response is therefore crucial, because persistent or unresolved inflammation can contribute to chronic non-healing wounds, while excessive or dysregulated repair may favor abnormal scarring[27].

The proliferative phase is characterized by the formation of new tissue to replace the damaged area and includes re-epithelialization, angiogenesis, fibroblast activation and ECM deposition. Keratinocytes located at the wound edge migrate and proliferate to restore epithelial continuity and re-establish the skin barrier, a process supported by growth factors such as EGF, KGF and TGF-α[26,31]. At the same time, fibroblasts migrate into the provisional matrix, proliferate and produce ECM proteins, including collagen, fibronectin and proteoglycans, contributing to the formation of granulation tissue[26]. Angiogenesis occurs in parallel and depends on endothelial cell activation, migration and proliferation, mainly in response to hypoxia-related and pro-angiogenic signals such as VEGF and FGFs[28]. The newly formed granulation tissue is rich in capillaries, fibroblasts and loose ECM, and provides temporary structural support for regenerating tissue[32].

The remodeling or maturation phase represents the final stage of wound repair and can continue for weeks, months or even years after wound closure[32]. During this phase, the initial granulation tissue is progressively reorganized into a more stable scar through ECM turnover, collagen fiber reorganization and changes in tissue vascularity[29]. Type III collagen, which is abundant in early granulation tissue, is gradually replaced by stronger type I collagen, while matrix metalloproteinases and their inhibitors regulate the balance between matrix degradation and deposition[28]. As metabolic demands decrease, newly formed blood vessels regress and the scar become relatively less vascular[26]. Although this process restores tissue continuity, adult skin repair generally results in scar formation rather than complete regeneration, and the repaired tissue rarely recovers the full strength, architecture and functionality of uninjured skin.

Overall, successful wound healing depends on the precise coordination of resident and infiltrating cells, extracellular matrix components, soluble mediators and mechanical cues. The extracellular matrix is not only a passive scaffold, but also regulates cell adhesion, migration, signaling and the availability of cytokines and growth factors during the repair process. When the balance between inflammation, matrix deposition, angiogenesis and

remodeling is disrupted, the healing process can shift toward pathological outcomes, such as chronic wounds, hypertrophic scars, keloids or fibrosis[28]. For this reason, understanding the cellular and molecular mechanisms underlying each phase of wound healing is essential for the development of more effective regenerative and therapeutic strategies.

2. AIM OF THE PROJECT

The aim of this work was to investigate the effects of blood-derived extracellular vesicles (EVs) on proliferation and wound healing capacity of primary human neonatal dermal fibroblasts. This work aimed to contribute to the understanding of the regenerative potential of blood-derived EVs and their possible application in tissue repair and regenerative medicine.

3. MATERIALS AND METHODS

3.1 EV ISOLATION

Extracellular vesicles (EVs) were isolated from peripheral blood obtained from a healthy donor. Blood samples were collected in EDTA tubes and centrifuged at 300×g for 10 min to separate the plasma fraction. The supernatant (plasma) was then transferred into ultracentrifuge tubes and filled with cold 1X phosphate-buffered saline (PBS).

Samples were subsequently centrifuged at 10,000×g for 30 min at 4 °C without brake using a Beckman Coulter Optima XPN-100 Ultracentrifuge (Beckman Coulter, Milan, Italy) to remove cellular debris and larger particles. The resulting supernatant was carefully transferred into new ultracentrifuge tubes, and the volume was adjusted with cold 1X PBS.

EVs were isolated by ultracentrifugation at 100,000×g for 2 hours at 4 °C without brake. After centrifugation, the supernatant was discarded and the pellet was resuspended in cold 1X PBS for a washing step. Samples were then subjected to a second ultracentrifugation at 100,000×g for 2 hours at 4 °C without brake. Finally, the supernatant was removed and the EV pellet derived from each blood collection tube was resuspended in 2 mL of 1X PBS for downstream experiments.

3.2 EV CHARACTERIZATION BY NANOPARTICLE TRACKING ANALYSIS

EVs were characterized and quantified by nanoparticle tracking analysis (NTA) using the NanoSight NS300 system (Malvern Panalytical, USA). This technique allowed the determination of particle size distribution and concentration by tracking the Brownian motion of particles suspended in solution through laser light scattering.

Measurements and marker characterization were performed at the Department of Molecular Biotechnology and Health Sciences, University of Turin. Samples were analyzed using a 488 nm blue laser and recordings were processed with NTA software, version 3.2 (NTA software solution, USA).

3.3 EV SURFACE MARKER ANALYSIS

EV surface marker characterization was performed using the MACSPlex Exosome Kit, human (Miltenyi Biotec, Bergisch Gladbach, Germany), according to the manufacturer's instructions. This assay enabled the simultaneous detection of 37 surface epitopes by flow cytometry using fluorescent bead-based technology. The kit contained 39 distinct bead populations, including 37 bead subsets coated with monoclonal antibodies specific for EV surface markers and 2 control bead populations.

For the analysis, 60 µL of isolated EVs were diluted with MACSPlex buffer (MPB) to a final volume of 120 µL. Subsequently, 15 µL of MACSPlex Exosome Capture Beads were added to each sample. To allow EV binding to the antibody-coated beads, the mixtures were incubated overnight at 4 °C on an orbital shaker at 450 rpm protected from light.

After incubation, EV–bead complexes were washed with 500 µL of MPB and centrifuged at 3000×g for 5 min at room temperature. After removing the supernatant, 5 µL each of APC-conjugated anti-CD9, anti-CD63, and anti-CD81 detection antibodies were added. The samples were then incubated for 1 hour at room temperature on an orbital shaker at 450 rpm, protected from light.

The samples were then washed with 500 µL of MPB and centrifuged at 3000×g for 5 min. A second washing step was performed using another 500 µL of MPB, followed by incubation on an orbital shaker at 450 rpm for 15 min at room temperature in the dark. Samples were then centrifuged again at 3000×g for 5 min, supernatant was removed, leaving approximately 150 µL for pellet resuspension.

Flow cytometry analysis was performed using a BD FACSCelesta flow cytometer (BD Biosciences, Franklin Lakes, NJ, USA). Background fluorescence derived from MACSPlex buffer and isotype controls was subtracted from each sample. Marker expression was expressed as median fluorescence intensity values.

3.4 PRIMARY FIBROBLAST CELL CULTURE

Primary human neonatal dermal fibroblasts (HDFn; ATCC PCS-201-010) were purchased from the American Type Culture Collection (ATCC, Manassas, VA, USA) and cultured in Dulbecco's Modified Eagle Medium high glucose (DMEM High Glucose; Aurogene, Italy) supplemented with 10% fetal bovine serum (FBS; Gibco, Thermo Fisher Scientific, USA) and 1% penicillin–streptomycin solution stabilized (Sigma-Aldrich, USA). Cells were maintained at 37 °C in a humidified atmosphere containing 5% CO_2. For routine cell culture maintenance, cells were detached using 0.25% trypsin-EDTA and centrifuged prior to reseeding. Cell number was determined using Trypan Blue staining and a Bürker counting chamber.

For experimental assays, primary fibroblasts were seeded in multiwell plates, 6 or 96 wells, and subsequently treated with different concentrations of EVs. Figure 3 shows a typical morphology of plated cells.

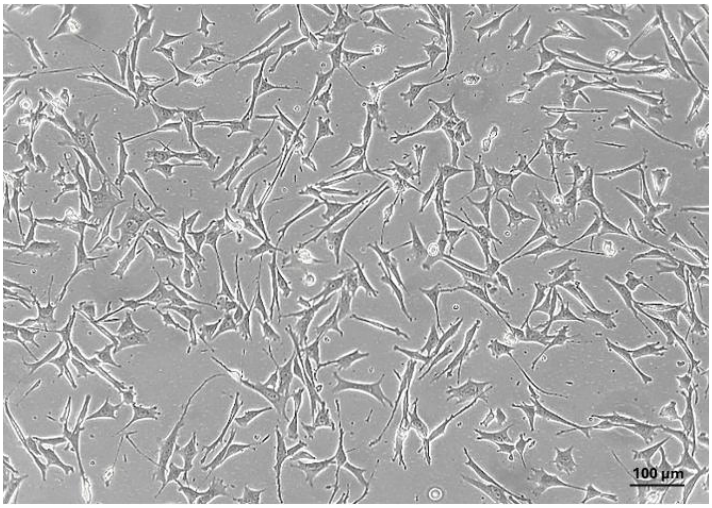

Figure 3 *- Primary fibroblasts cultured in our laboratory, observed under light microscopy (200x).*

3.5 INCUCYTE® LIVE-CELL PROLIFERATION ASSAY

Primary fibroblasts were seeded in 96-well plates at a density of 500 cells/well in a final volume of 100 µL of complete culture medium. After 24 hours, the culture medium was removed and replaced with different experimental conditions.

Cells cultured in DMEM supplemented with 10% FBS were used as positive control (CT+), while cells cultured in serum-free DMEM were used as negative control (CT-). Extracellular vesicles were quantified and the final concentration resulted 2.98×10^8 particles/mL and were tested

on cells at different dilutions (1:4, 1:6, 1:8, 1:10, 1:12, and 1:16), prepared in DMEM containing 10% FBS and serum-free DMEM. Positive and negative controls were tested in 12 replicates, whereas each EV treatment condition was tested in 6 replicates.

Following treatment, the plate was placed into the Incucyte® Live-Cell Analysis System for live-cell imaging analysis. Cell proliferation was monitored for a total of 66 hours, with image acquisition performed every 6 hours. For each well, 9 images were acquired at each time point.

3.6 INCUCYTE® LIVE-CELL WOUND HEALING ASSAY

For wound healing experiments, primary fibroblasts were seeded in 96-well plates at a density of 20,000 cells/well in a final volume of 100 µL in order to obtain a complete cell monolayer. After 24 hours, cells reached 90% confluence and a scratch was simultaneously generated in each well using the Incucyte® 96-well Woundmaker Tool provided with the Incucyte® Live-Cell Analysis System.

Following scratch generation, the culture medium was removed, and cells were washed once with 1X PBS. Subsequently, different treatment conditions were added. Based on the results obtained from the proliferation assay, only the most significant experimental conditions were selected for the wound healing assay. DMEM supplemented with 10% FBS was used as positive control (CT+), while serum-free DMEM was used as negative control (CT-). Extracellular vesicles diluted 1:8 and 1:10 in DMEM with or without FBS were tested.

After treatment, the plate was placed into the Incucyte® system for live-cell imaging analysis. Wound closure was monitored automatically for 27 hours through sequential image acquisition performed every 3 hours. Twelve replicates were included for each experimental condition.

3.7 RNA ISOLATION

Fibroblasts were seeded in 6-well plates at a density of 8×10^4 cells per well. After 24 hours, the culture medium was removed and replaced with the corresponding treatment media. Cells were exposed to EVs at 1:8 and 1:10 dilutions in either DMEM supplemented with 10% FBS or serum-free DMEM, using the same experimental conditions adopted for the wound healing assay. DMEM supplemented with 10% FBS and serum-free DMEM were used as positive and

negative controls. After 24 h of treatment, the stimulation medium was removed, and cells were lysed directly in the wells using 500 µL of TRI Reagent® solution (Zymo Research, Irvine, CA, USA). This method enables the simultaneous isolation of RNA, DNA, and proteins from the same biological sample. Total RNA was extracted according to the manufacturer's instructions and was used for the analyses described in this thesis, while the protein fraction was collected and stored at −80 °C for future studies. Following extraction, RNA concentration and purity were assessed using a NanoDrop ND-1000 UV-Vis spectrophotometer.

3.8 REVERSE TRANSCRIPTION

Total RNA was reverse transcribed into complementary DNA (cDNA) using the GoScript™ Reverse Transcription System (Promega, Milan, Italy) according to the manufacturer's instructions. Prior to reverse transcription, RNA concentration was determined by spectrophotometric analysis and samples were normalized to ensure comparable RNA input. Approximately 0.64 µg of total RNA was used for each reaction.

For each sample, total RNA was combined with 0.5 µg of Random Primers and nuclease-free water to a final volume of 5 µL. Reverse transcription reactions were performed in a final volume of 20 µL, consisting of 5 µL of RNA/primer mix and 15 µL of reaction mixture. The composition of the reaction mixture is reported in the following table.

Table 1 *- Composition of the reverse transcription reaction mixture used for cDNA synthesis.*

Component	**Volume (1 reaction)**
Nuclease-free water	7.8 µL
GoScript™ 5X Reaction Buffer	4 µL
$MgCl_2$	1.2 µL
PCR Nucleotide Mix	1 µL
GoScript Reverse Transcriptase	1 µL
Final Volume	**15 µL**

The resulting cDNA was subsequently used for gene expression analyses.

3.9 QUANTITATIVE REAL-TIME PCR

Quantitative real-time PCR (qRT-PCR) was performed using the SsoAdvanced™ Universal SYBR® Green Supermix (Bio-Rad, Hercules, CA, USA). Amplification reactions were prepared in a final volume of 20 µL containing 10 µL of SsoAdvanced™ Universal SYBR® Green Supermix (2X), 1 µL of cDNA template obtained from the reverse transcription reaction, 1 µL each of forward and reverse primers (final concentration 500 nM), and 7 µL nuclease-free water.

Gene expression analysis was performed for selected genes associated with proliferation, cell cycle regulation and inflammatory response, including KI67, CDKN1A, TLR7 and IL6. ACTB (β-actin) was used as the reference gene for normalization. Primer sequences are reported in Table 2.

Amplification reactions were carried out using a CFX96 Real-Time PCR Detection System according to the thermal cycling conditions reported in Table 3.

Table 2 *- Primer sequences used for qRT-PCR analysis. ACTB: actin beta, used as housekeeping gene for normalization; CDKN1A: cyclin-dependent kinase inhibitor 1A, also known as p21, involved in cell-cycle regulation.*

Gene	Primer type	Sequence (5'→3')
ACTB	Forward	CGAAGCCGGCCTTGCACAT
ACTB	Reverse	GCACAGAGCCTCGCCTTTG
CDKN1A	Forward	AGGTGGACCTGGAGACTCTCAG
CDKN1A	Reverse	TCCTCTTGGAGAAGATCAGCCG
TLR7	Forward	CTTTGGACCTCAGCCACAACCA
TLR7	Reverse	CGCAACTGGAAGGCATCTTGTAG
KI67	Forward	GAAAGAGTGGCAACCTGCCTTC
KI67	Reverse	GCACCAAGTTTTACTACATCTGCC
IL6	Forward	AGACAGCCACTCACCTCTTCAG
IL6	Reverse	TTCTGCCAGTGCCTCTTTGCTG

Table 3 *- Thermal cycling protocol. SYBR® Green: fluorescent double-stranded DNA-binding dye used to monitor PCR amplification during qRT-PCR*

		Amplification			
Setting	**Polymerase Activation and DNA Denaturation**	**Denaturation at 95 °C**	**Annealing/Extension and Plate Read at 60 °C**	**Cycles**	**Melt Curve Analysis**
SYBR® green	30 sec at 98 °C	15 sec	30 sec	40	65-95 °C 0.5 °C increments at 5 sec/step

3.10 STATISTICAL ANALYSIS

Data are presented as mean ± SEM. Statistical analyses were performed using two-way ANOVA followed by multiple comparison tests using GraphPad Prism version 11.0.2 (GraphPad Software, San Diego, CA, USA). Differences were considered statistically significant at $p < 0.05$. Statistical significance was indicated as follows: *=p<0.05, **=p<0.01, ***=p<0.001, ****=p<0.0001.

4. RESULTS

4.1 NTA CHARACTERIZATION RESULTS

Nanoparticle tracking analysis (NTA) revealed a heterogeneous population of extracellular vesicles with a predominant size distribution compatible with small EVs. The average particle diameter was 140.6 nm, while the modal size was 95.5 nm, indicating that the majority of vesicles were within the expected range for small extracellular vesicles[33]. In addition, the particle concentration was estimated at 2.98×10^8 particles/mL (Figure 4).

The size distribution profile showed a main peak between 90 and 120 nm, together with a smaller population of larger particles, which is commonly observed in plasma-derived EV preparations (Figure 4). These results confirmed the successful isolation of EVs suitable for downstream in vitro experiments.

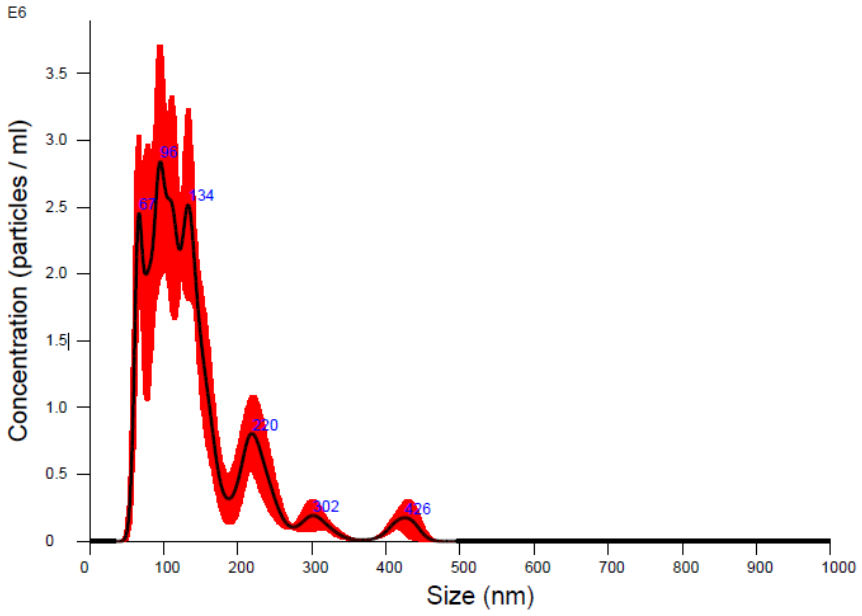

Figure 4 *- Size distribution of plasma-derived EVs measured by nanoparticle tracking analysis (NTA). The analysis showed a predominant population of particles within the small EV size range, with a modal size of 95.5 nm and a mean diameter of 140.6 nm. Error bars represent +/- SEM.*

4.2 SURFACE MARKER ANALYSIS RESULTS

Flow cytometry analysis using the MACSPlex Exosome Kit revealed the presence of EVs expressing a variety of surface markers. Dot plot analysis confirmed the successful detection of EV-associated bead populations based on scatter properties and APC fluorescence intensity (Figure 5). Among the 37 markers analyzed, EVs showed expression of the canonical

tetraspanin markers CD9, CD63, and CD81. CD42a exhibited the highest median fluorescence intensity, followed by CD62P and CD49e (Figure 6). The high expression of platelet-associated markers, particularly CD42a and CD62P, suggests that a large proportion of the analyzed EVs may be platelet-derived, which is consistent with the plasma origin of the sample. Additional markers, including CD3, CD56, CD29, and CD31, were also detected, indicating the heterogeneous surface marker profile of the analyzed EV population.

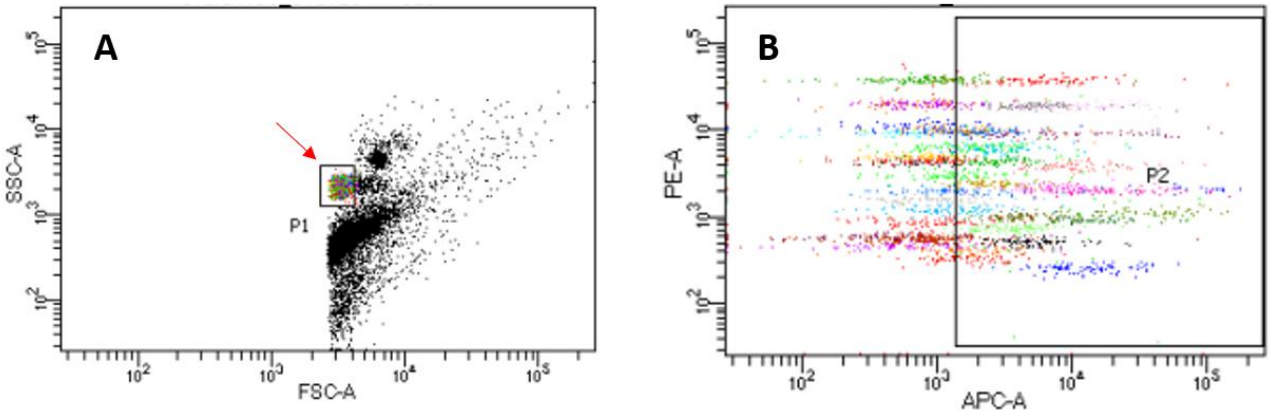

Figure 5 *- Panel A shows distribution of events based on size (Forward Scatter, FSC-A) and granularity (Side Scatter, SSC-A). Gate P1 isolates the homogeneous population of single microspheres based on their physical properties, excluding background debris and bead aggregates from downstream analysis. Panel B shows fluorescence profile applied exclusively to the events pre-selected in gate P1. The X-axis (Allophycocyanin, APC) displays the separation of distinct bead regions. The Y-axis (Phycoerythrin, PE) measures the signal intensity of the fluorescent detection antibody. Gate P2 defines the region for target analyte quantification.*

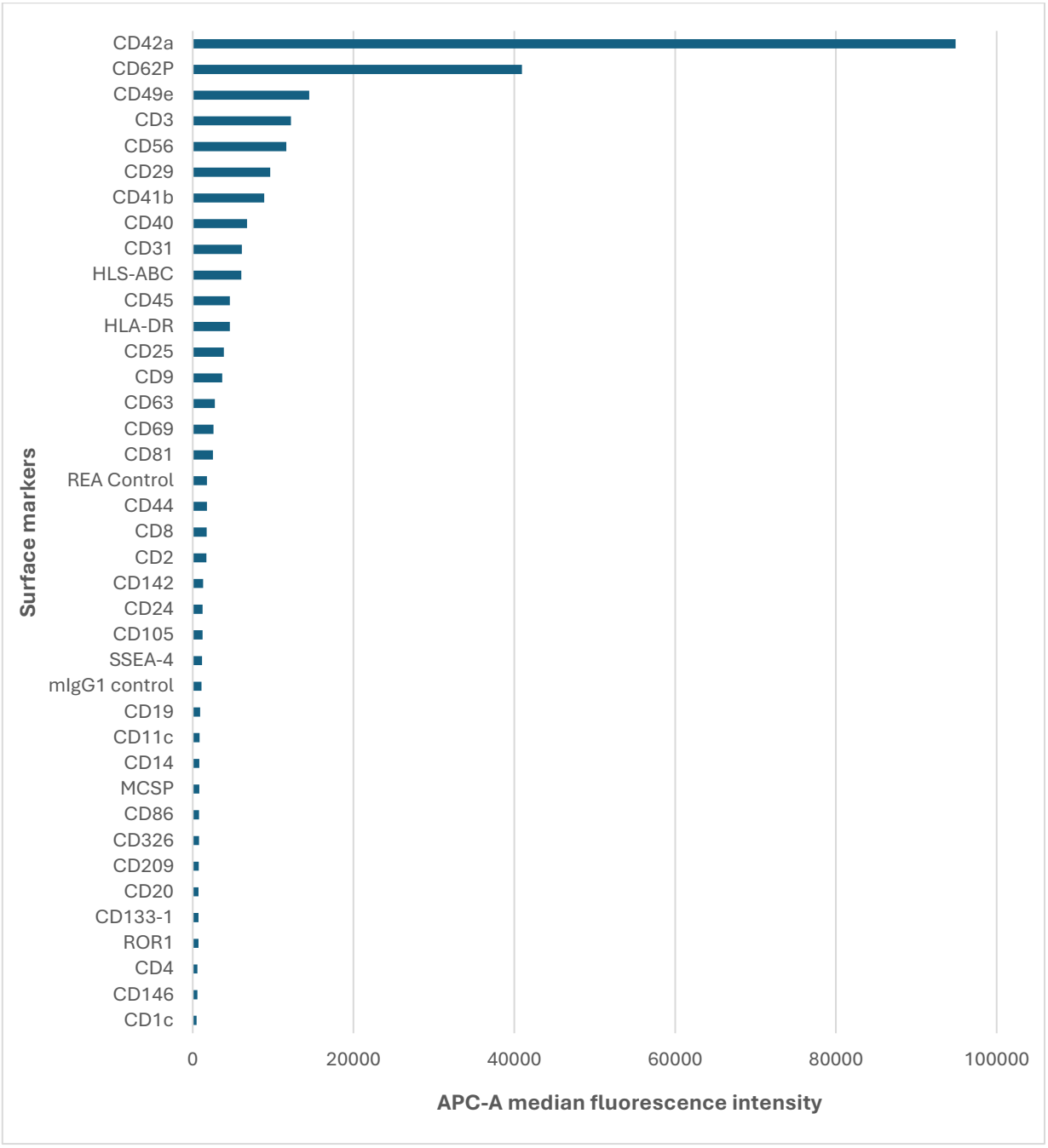

Figure 6 *- Surface marker profile of isolated extracellular vesicles determined by MACSPlex analysis. Marker expression is reported as median fluorescence intensity.*

4.3 INCUCYTE® PROLIFERATION ASSAY RESULTS

The proliferation of primary fibroblasts was first assessed under control conditions by comparing cells cultured in complete medium (CT+) with cells maintained in serum-free medium (CT−). As shown in Figure 7, both conditions displayed a progressive increase in Δ confluency over time; however, CT+ cells showed a markedly higher increase compared with

CT− cells. A statistically significant difference between the two control conditions was observed starting from 12 hours, with stronger significance detected at later time points.

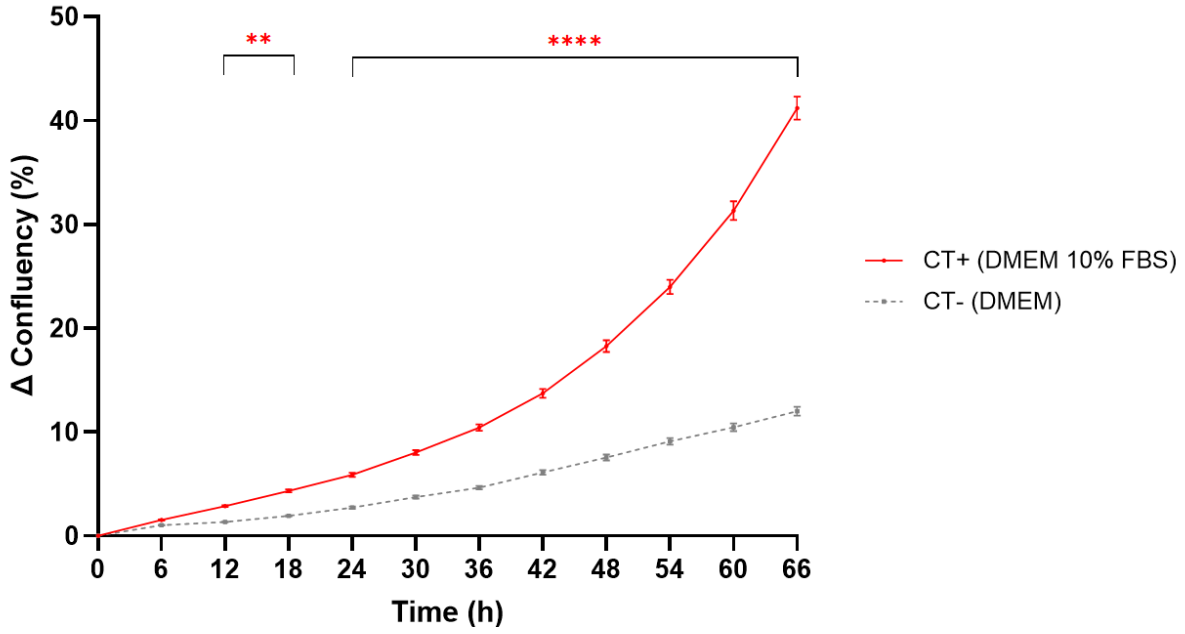

Figure 7 *- Proliferation profile of primary human dermal fibroblasts under control conditions. Fibroblast proliferation was evaluated over 66 hours and expressed as Δ confluency (%), calculated by subtracting the corresponding T0 value from each time point. Cells cultured in complete medium (CT+; DMEM supplemented with 10% FBS) showed a progressive increase in confluency compared with cells cultured in serum-free medium (CT-; DMEM). Data are reported as mean ± SEM. Statistical significance refers to the comparison between CT+ and CT− at the indicated time points; **=p<0.01, ****=p < 0.0001.*

EV-treated conditions were then analyzed separately according to the presence or absence of FBS. In FBS-supplemented medium (FBS+), EV-treated fibroblasts showed different trends depending on the EV dilution. All tested conditions displayed a progressive increase in Δ confluency over time, with values generally comparable to or higher than the positive control. Among the tested dilutions, EV 1:10 FBS+ showed the highest Δ confluency values at several time points, including the final time point (Figure 8).

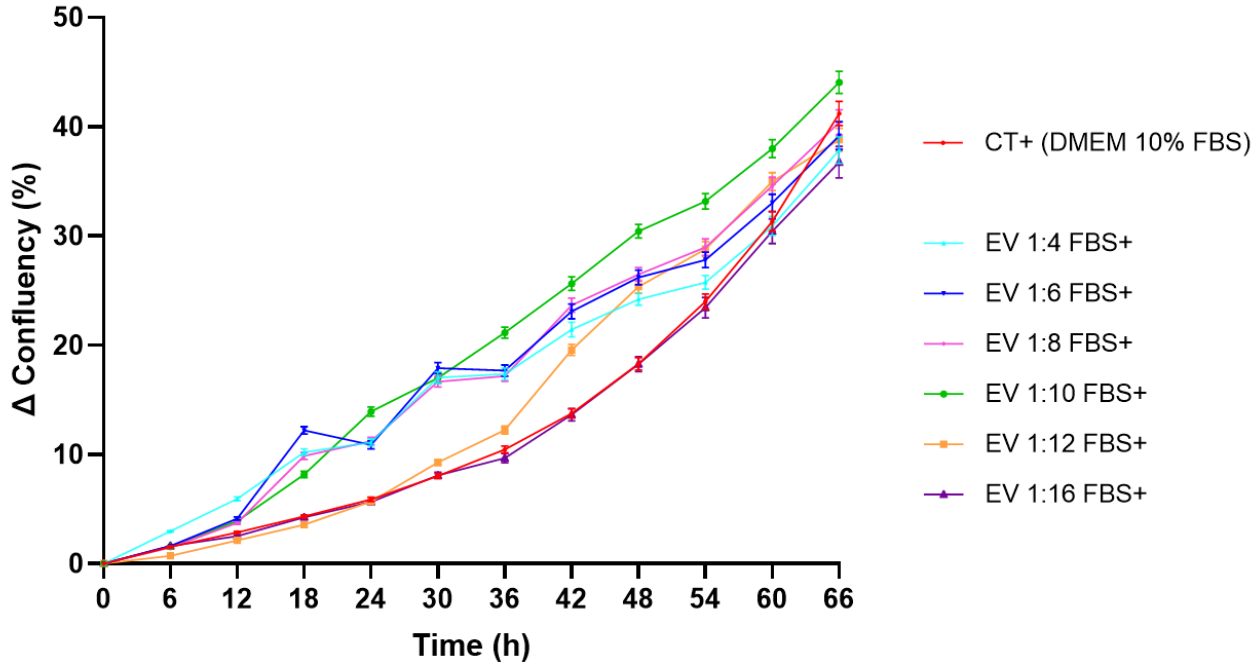

Figure 8 *- Proliferation profile of primary human dermal fibroblasts treated with EVs in complete medium. Fibroblast proliferation was evaluated over 66 hours and expressed as Δ confluency (%), calculated by subtracting the corresponding T0 value from each time point. EVs were tested at different dilutions (1:4, 1:6, 1:8, 1:10, 1:12 and 1:16) in DMEM supplemented with 10% FBS and compared with the positive control (CT+; DMEM supplemented with 10% FBS). Data are reported as mean ± SEM.*

Statistical analysis was performed with two-way ANOVA, followed by Dunnett's multiple comparison test, to compare each EV-treated condition with CT+. Significant differences were observed at multiple time-points, as reported in Table 4.

Table 4 *– The table summarizes the statistical analyses of fibroblast proliferation after EV treatment in complete medium. Statistical comparisons were made between the positive control (CT+; DMEM supplemented with 10% FBS) and each of the EV-treated condition prepared in complete medium (FBS+). Significance was evaluated at selected time points during the proliferation assay. ns: not significant; *=p<0.05; **=p<0.01; ***=p<0.001; ****=p<0.0001.*

Condition	12h	24h	36h	48h	66h
CT+ vs 1:4 FBS+	***	****	****	****	***
CT+ vs 1:6 FBS+	ns	****	****	****	ns
CT+ vs 1:8 FBS+	ns	****	****	****	ns
CT+ vs 1:10 FBS+	ns	****	****	****	**
CT+ vs 1:12 FBS+	ns	ns	ns	****	*
CT+ vs 1:16 FBS+	ns	ns	ns	ns	****

In serum-free medium (FBS−), all conditions showed a progressive increase in Δ confluency over time. Most EV-treated conditions reached higher values than CT−, especially EV 1:8 FBS−

and EV 1:10 FBS−, which showed the highest Δ confluency values at the final time point. By contrast, EV 1:4 FBS− was the only condition showing lower values than CT− (Figure 9).

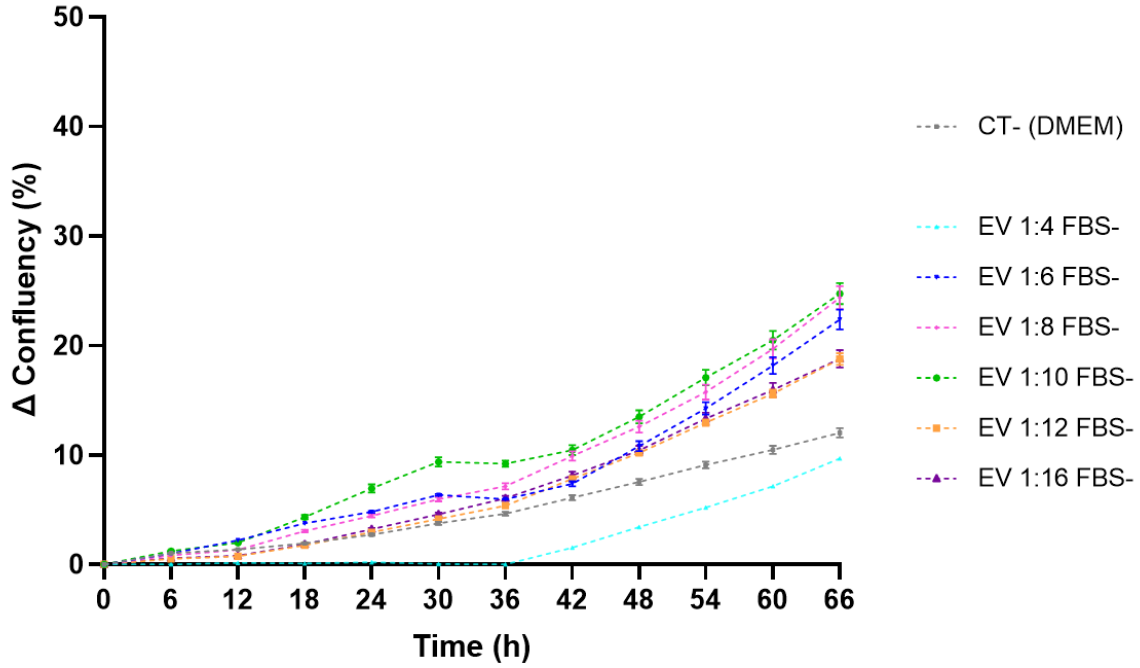

Figure 9 *- Proliferation profile of primary human dermal fibroblasts treated with EVs in serum-free medium. Fibroblast proliferation was evaluated over 66 hours and expressed as Δ confluency (%), calculated by subtracting the corresponding T0 value from each time point. EVs were tested at different dilutions (1:4, 1:6, 1:8, 1:10, 1:12 and 1:16) in serum-free DMEM and compared with the negative control (CT-; serum-free DMEM). Data are reported as mean ± SEM.*

The statistical analysis was performed with two-way ANOVA and Dunnett's multiple comparison test to compare each EV-treated condition (FBS-) with CT−.

Significant differences were observed at multiple time points and reported in Table 5

Table 5 *– The table summarizes the statistical analysis of fibroblast proliferation after EV treatment in serum-free medium. Statistical comparisons were performed between the negative control (CT-; serum-free DMEM) and each of the EV-treated condition prepared in serum-free medium (FBS-). Significance was evaluated at selected time points during the proliferation assay. ns: not significant; *=p<0.05; **=p<0.01; ***=p<0.001; ****=p<0.0001.*

Condition	12h	24h	36h	48h	66h
CT- vs 1:4 FBS-	*	****	****	****	****
CT- vs 1:6 FBS-	ns	****	*	****	****
CT- vs 1:8 FBS-	ns	**	****	****	****
CT- vs 1:10 FBS-	ns	****	****	****	****
CT- vs 1:12 FBS-	ns	ns	ns	****	****
CT- vs 1:16 FBS-	ns	ns	*	****	****

Overall, EV treatment influenced fibroblast proliferation over time, with effects varying according to EV dilution and culture condition.

4.4 INCUCYTE® WOUND HEALING ASSAY RESULTS

Wound closure was evaluated over 27 hours and expressed as wound confluence (%). Control conditions showed distinct wound closure profiles, with CT+ displaying a progressive increase in wound confluence over time compared with CT-. At the final time point, CT+ reached a higher wound confluence than CT-, confirming the expected difference between complete and serum-free culture conditions (Figure 10).

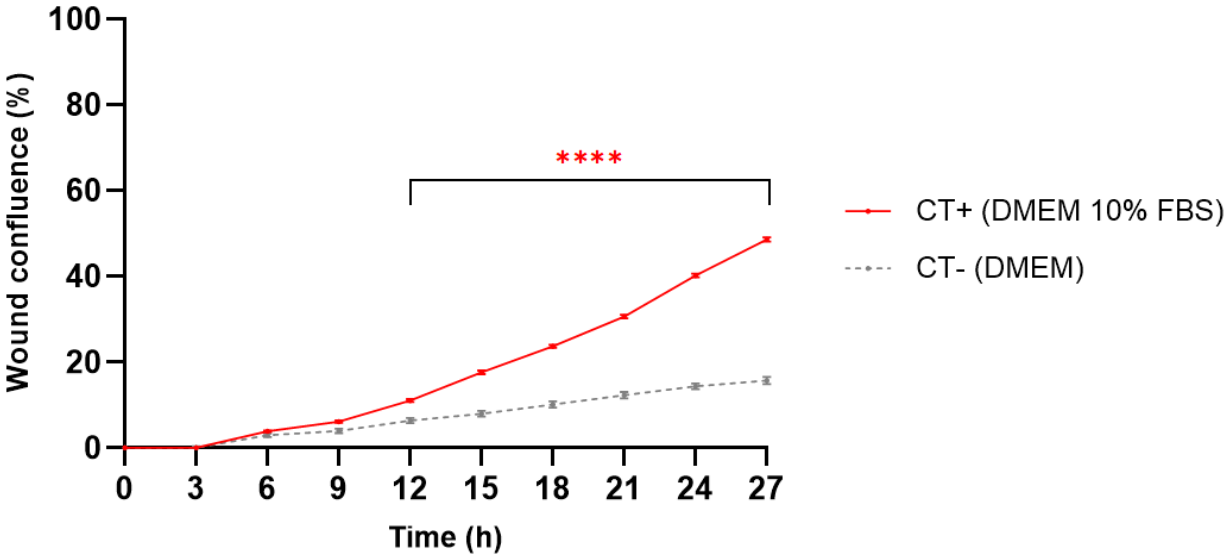

Figure 10 *- Wound closure profile of primary human dermal fibroblasts under control conditions. Wound closure was monitored over 27 hours and expressed as wound confluence (%). Cells cultured in complete medium (CT+; DMEM supplemented with 10% FBS) showed a progressive increase in wound confluence compared with cells cultured in serum-free medium (CT-; DMEM). Data are reported as mean ± SEM. Statistical significance refers to the comparison between CT+ and CT− at the indicated time points; ****=p < 0.0001.*

Based on the proliferation assay results, EV dilutions 1:8 and 1:10 were selected for the wound healing assay and analyzed separately in the presence or absence of FBS. In complete medium, fibroblasts treated with EVs at both 1:8 and 1:10 dilutions showed a higher wound confluence compared with CT+ over time. Statistical analysis showed significant differences between EV-treated conditions and CT+ at selected time points, as indicated in the graph (Figure 11).

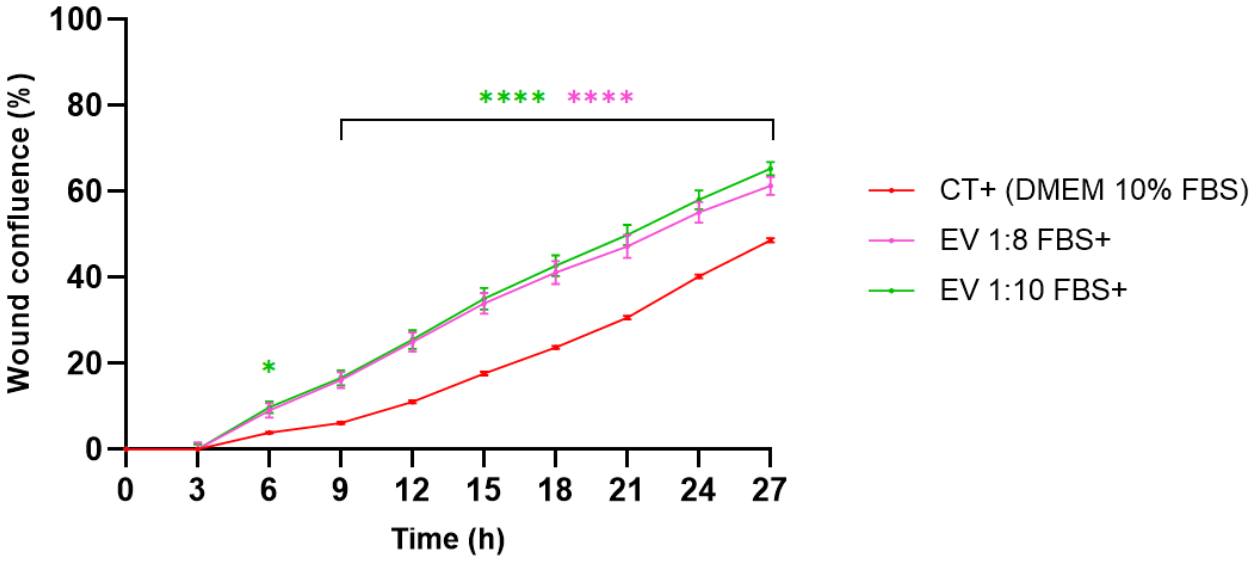

Figure 11 *- Wound closure profile of primary human dermal fibroblasts treated with EVs in complete medium. Wound closure was monitored over 27 hours and expressed as wound confluence (%). Fibroblasts were treated with EVs at 1:8 and 1:10 dilutions in DMEM supplemented with 10% FBS (FBS+) and compared with the positive control (CT+; DMEM supplemented with 10% FBS). Data are reported as mean ± SEM. Statistical significance was evaluated by comparing each EV-treated condition with CT+; significance is indicated in the graph (*=p<0.05; ****=p<0.0001).*

In serum-free medium, EV-treated fibroblasts also showed increased wound closure compared with CT-. Both 1:8 and 1:10 EV dilutions displayed a progressive increase in wound confluence over time, with statistically significant differences compared with CT- at several time points (Figure 12).

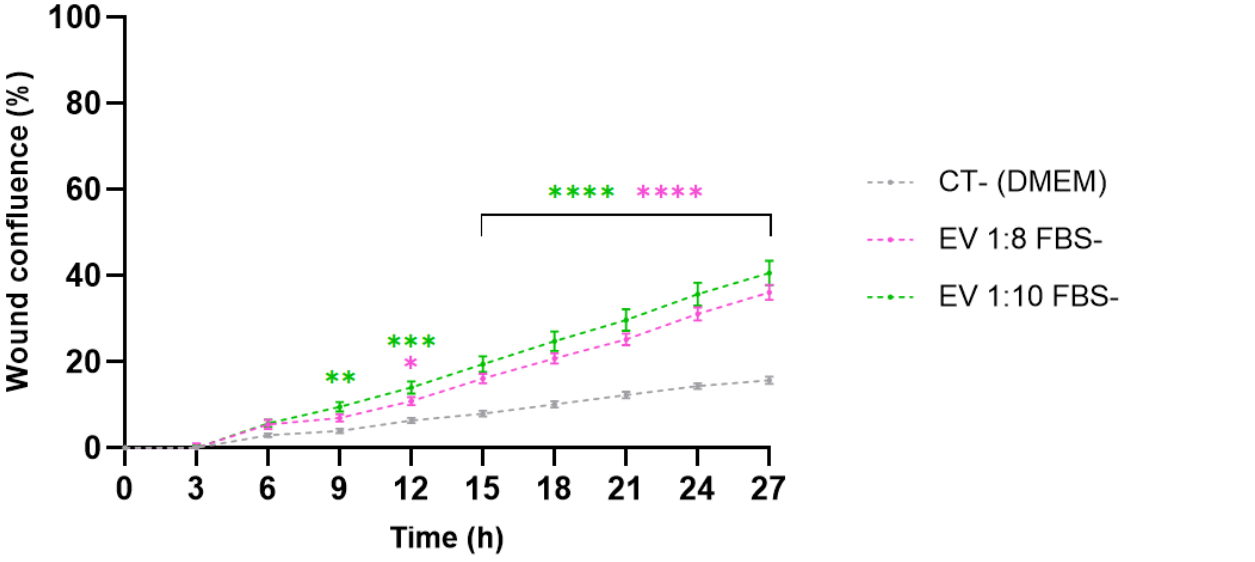

Figure 12 *- Wound closure profile of primary human dermal fibroblasts treated with EVs in serum-free medium. Wound closure was monitored over 27 hours and expressed as wound confluence (%). Fibroblasts were treated with EVs at 1:8 and 1:10 dilutions in serum-free DMEM (FBS-) and compared with the negative control (CT-; DMEM). Data are reported as mean ± SEM. Statistical significance was evaluated by comparing each EV-treated condition with CT-; significance is indicated in the graph (*=p<0.05; **=p<0.01; ***=p<0.001; ****=p<0.0001).*

Representative Incucyte® images showed a progressive reduction of the wound area over time, confirming the wound closure trend observed under the different experimental conditions (Figure 13 and Figure 14).

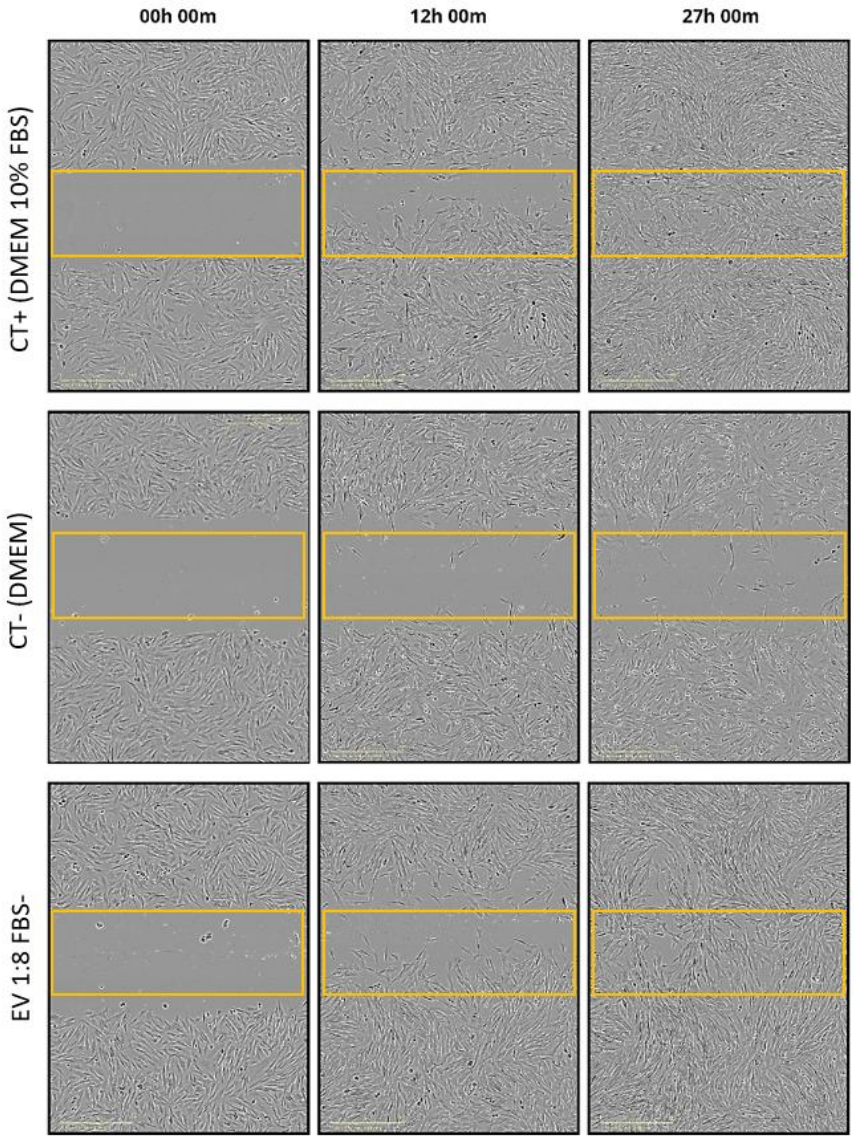

Figure 13 *- Representative Incucyte® images of the wound healing assay under control and EV-treated conditions. Representative phase-contrast images of primary human dermal fibroblasts acquired at 0, 12 and 27 hours after scratch generation. Images show wound closure under complete medium (CT+; DMEM supplemented with 10% FBS), serum-free medium (CT-; DMEM) and EV treatment at 1:8 dilution in serum-free DMEM. The images qualitatively illustrate wound closure progression over time. Yellow box indicates the area where wound analysis was performed.*

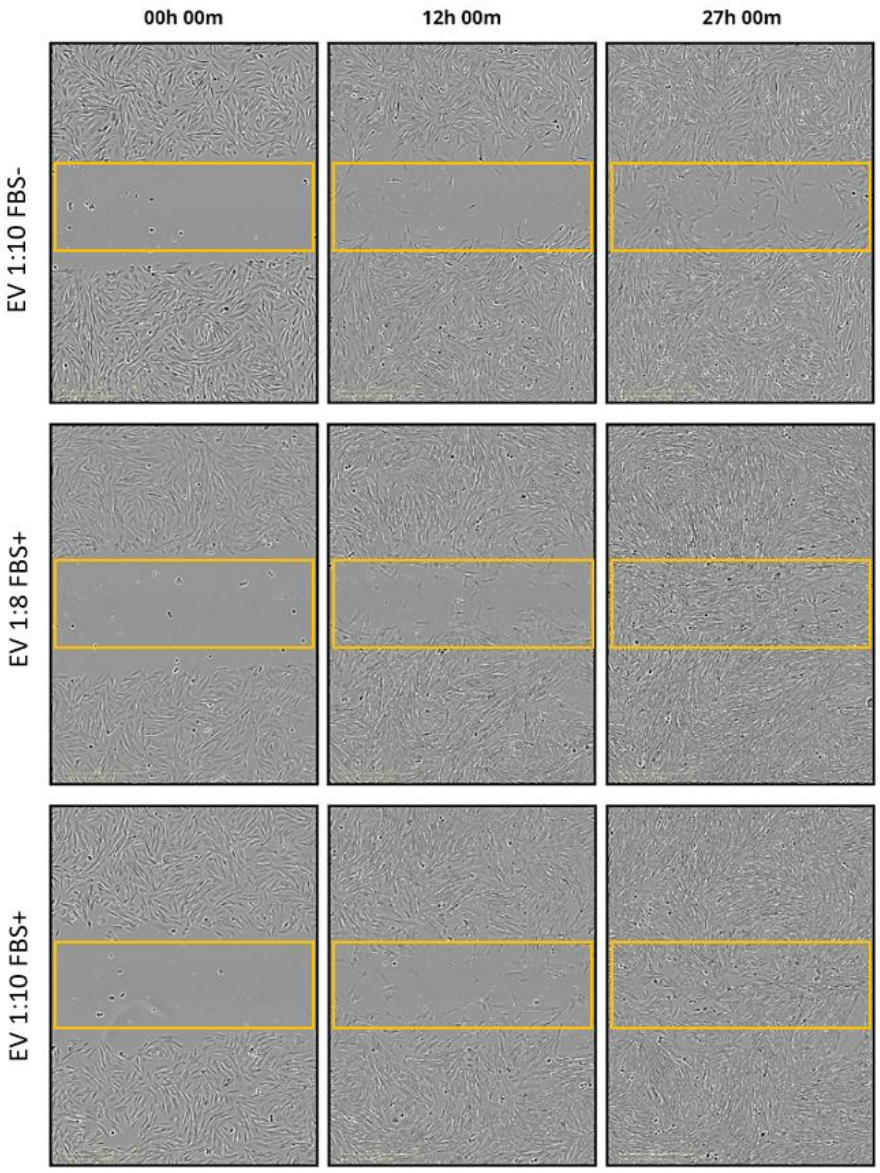

Figure 14 *- Representative Incucyte® images of the wound healing assay under EV-treated conditions. Representative phase-contrast images of primary human dermal fibroblasts acquired at 0, 12 and 27 hours after scratch generation. Images show wound closure after treatment with EVs at 1:10 dilution in serum-free DMEM and at 1:8 or 1:10 dilutions in DMEM supplemented with 10% FBS. The images qualitatively illustrate wound closure progression over time. Yellow box indicates the area where wound analysis was performed.*

4.5 q-PCR RESULTS

Gene expression analysis was performed to further evaluate the response of fibroblasts to EV treatment. Among the selected target genes, KI67, TLR7 and IL6 were undetected under the analyzed experimental conditions and were therefore not included in the subsequent quantitative analysis. For this reason, only CDKN1A expressions were evaluated. As shown in Figure 15, CDKN1A expression showed only limited variation among the analyzed conditions. EV 1:8-treated cells showed a slight increase in CDKN1A expression under both FBS+ and FBS-

conditions. In contrast, EV 1:10-treated cells showed minor changes compared with their respective controls, with opposite trends depending on the presence or absence of FBS. However, no statistically significant differences were observed between EV-treated cells and the corresponding control conditions.

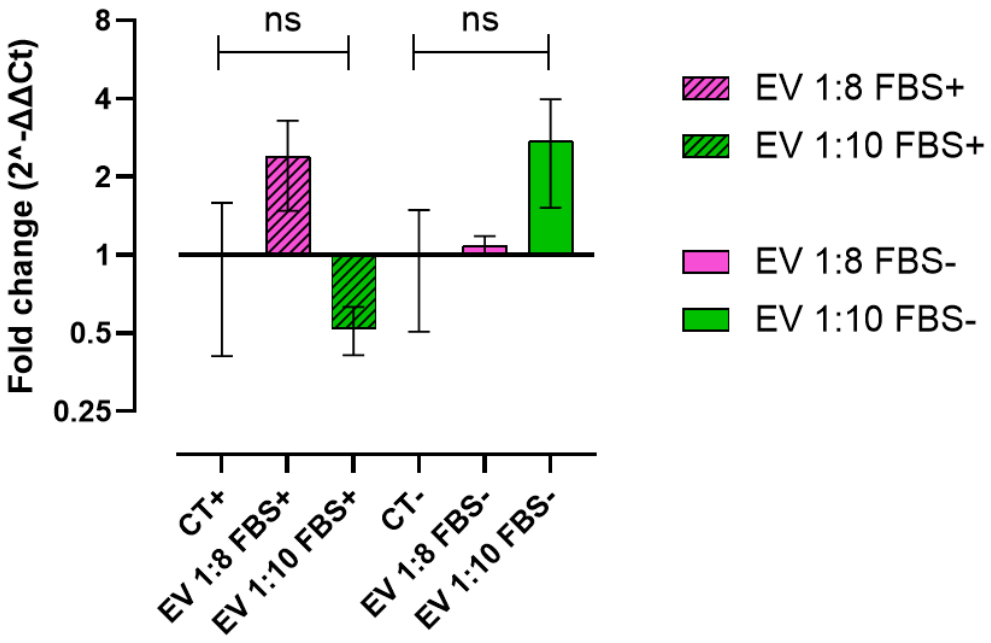

Figure 15 *- Relative expression of CDKN1A in EV-treated primary human dermal fibroblasts. CDKN1A gene expression was evaluated by qRT-PCR in fibroblasts treated with EV 1:8 and EV 1:10 under FBS-supplemented (FBS+) and serum-free (FBS-) conditions. EV treatments prepared in FBS+ medium were compared with the FBS-supplemented control (CT+), whereas EV treatments prepared in FBS− medium were compared with the serum-free control (CT−). The y-axis reports CDKN1A fold change after normalization to ACTB (β-actin), with the corresponding control condition set to 1 in each comparison. Data are reported as mean ± SD. No statistically significant differences were observed. ns, not significant.*

5. DISCUSSION

Nanoparticle tracking analysis confirmed the presence of a heterogeneous population of particles with a size distribution mainly compatible with small extracellular vesicles, although the broader distribution and the presence of minor peaks corresponding to larger particles indicated that the preparation was not completely homogeneous. This finding is expected for plasma-derived EV preparations, since plasma is a complex biological fluid containing vesicles released by multiple cell types, together with other circulating nanosized components. However, because NTA does not distinguish EVs from non-vesicular particles, such as protein aggregates or lipoproteins, these data should be interpreted together with surface marker analysis.

The MACSPlex analysis provided additional characterization of the isolated EV population by evaluating the expression of multiple surface markers. The detection of canonical EV-associated tetraspanins, including CD9, CD63 and CD81, supported the presence of extracellular vesicles in the analyzed preparation. The analyses showed that there was a CD42a fraction that is associated with platelet origin and CD62P that is related to platelet activation[34]. The detection of CD49e, corresponding to integrin α5, indicates the presence of adhesion-related surface molecules within the EV population. Additional markers, such as CD3, CD56, CD29 and CD31, further support the heterogeneous origin of the isolated EV population, suggesting contributions from different cell types, including T lymphocytes, natural killer cells, endothelial/platelet-associated populations, and cells expressing adhesion-related integrins.

The proliferation assay performed with Incucyte® instrument showed that blood-derived EVs were able to modulate fibroblast proliferation rate over time. This effect varied according to EV dilution in a dose dependent manner and the presence or absence of serum-derived factors. In complete medium with 10 % FBS, EV treatment appeared to further influence cell growth, suggesting a possible synergy between EV-associated bioactive signals and serum-derived factors. These data indicate that, in presence of serum, blood-derived EVs may act as additional modulators of fibroblast proliferation rather than a sole source of proliferative stimulation.

Our results indicate that the 1:8 and 1:10 dilutions were able to boost the proliferative ability of the cells, in both serum or serum-free conditions. In serum-free conditions, the effect of EVs

on fibroblast proliferation was particularly relevant from a biological point of view, because it was observed in the absence of external serum-derived growth factors. The ability of some EV-treated conditions to partially compensate for serum withdrawal suggests that blood-derived EVs may carry bioactive signals capable of supporting fibroblast growth. This reinforces the idea that EVs can act as endogenous mediators involved in fibroblast activation and tissue repair.

Based on the proliferation assays, the most promising EV dilutions, 1:8 and 1:10, were selected for the wound healing experiments. In this functional model, EV-treated fibroblasts showed an improved wound closure profile compared with the respective control conditions, suggesting that blood-derived EVs may enhance fibroblast activities involved in the repair process. This observation is consistent with the known role of blood-derived and platelet-associated EVs as carriers of bioactive molecules involved in cell activation, adhesion, proliferation and tissue remodeling.

The qRT-PCR analysis was performed to further investigate whether the functional effects observed in the Incucyte® assays were associated with changes in the expression of some genes related to proliferation, cell-cycle regulation and inflammatory response. However, among the selected target genes, KI67, IL6 and TLR7 were undetected under the analyzed experimental conditions, limiting the molecular interpretation of the fibroblast response to EV treatment. For this reason, the analysis was focused on CDKN1A, a gene involved in cell-cycle regulation. CDKN1A expression showed only limited and non-significant variation among the analyzed conditions, without a clear treatment-dependent modulation. This suggests that the effects observed in the proliferation and wound healing assays were not associated with a marked transcriptional regulation of CDKN1A at the analyzed time point. These data need to be further exploited due to the limited number of experiments carried out and the limited statistical significance. Overall, these findings indicate that the functional response of fibroblasts to blood-derived EVs may not be directly reflected by changes in the selected gene expression markers. This could be due to several factors, including the timing of RNA collection, the limited number of genes analyzed, or the possibility that EV-mediated effects involve other molecular pathways not investigated in this study. Therefore, additional analyses, including different time points, a broader panel of genes and protein-level evaluation, would be necessary to better clarify the mechanisms underlying the observed biological effects.

6. CONCLUSIONS AND LIMITATIONS OF THE STUDY

In conclusion, the data, taken as a whole, support the hypothesis that EVs can have effects on some cell type. We have shown that characterized human blood derived EVs can play a relevant role in regenerative ability of primary human fibroblasts in different conditions and in absence of important physiological stimuli like serum. This study is preliminary and is limited by the number of experimental conditions. More data is necessary to understand if the proliferative capacity is linked to direct modulation of cell biochemistry or gene expression, and if gender, age and pathological conditions might affect this property.

7. BIBLIOGRAPHY

1. Visnovitz, T. (2024). Extracellular Vesicles: Biology and Therapeutic Applications. Preprint at Multidisciplinary Digital Publishing Institute (MDPI), https://doi.org/10.3390/ijms252313034 https://doi.org/10.3390/ijms252313034.

2. Xiong, L., Wei, Y., Jia, Q., Chen, J., Chen, T., Yuan, J., Pi, C., Liu, H., Tang, J., Yin, S., et al. (2023). The application of extracellular vesicles in colorectal cancer metastasis and drug resistance: recent advances and trends. Preprint at BioMed Central Ltd, https://doi.org/10.1186/s12951-023-01888-1 https://doi.org/10.1186/s12951-023-01888-1.

3. Yang, C., Xue, Y., Duan, Y., Mao, C., and Wan, M. (2024). Extracellular vesicles and their engineering strategies, delivery systems, and biomedical applications. Preprint at Elsevier B.V., https://doi.org/10.1016/j.jconrel.2023.11.057 https://doi.org/10.1016/j.jconrel.2023.11.057.

4. Hu, Y., Rao, S.S., Wang, Z.X., Cao, J., Tan, Y.J., Luo, J., Li, H.M., Zhang, W.S., Chen, C.Y., and Xie, H. (2018). Exosomes from human umbilical cord blood accelerate cutaneous wound healing through miR-21-3p-mediated promotion of angiogenesis and fibroblast function. Theranostics *8*, 169–184. https://doi.org/10.7150/thno.21234.

5. Dang, X.T.T., Kavishka, J.M., Zhang, D.X., Pirisinu, M., and Le, M.T.N. (2020). Extracellular Vesicles as an Efficient and Versatile System for Drug Delivery. Preprint at NLM (Medline), https://doi.org/10.3390/cells9102191 https://doi.org/10.3390/cells9102191.

6. Kumar, M.A., Baba, S.K., Sadida, H.Q., Marzooqi, S. Al, Jerobin, J., Altemani, F.H., Algehainy, N., Alanazi, M.A., Abou-Samra, A.B., Kumar, R., et al. (2024). Extracellular vesicles as tools and targets in therapy for diseases. Preprint at Springer Nature, https://doi.org/10.1038/s41392-024-01735-1 https://doi.org/10.1038/s41392-024-01735-1.

7. van der Pol, E., Böing, A.N., Harrison, P., Sturk, A., and Nieuwland, R. (2012). Classification, functions, and clinical relevance of extracellular vesicles. Pharmacol. Rev. *64*, 676–705. https://doi.org/10.1124/pr.112.005983.

8. Sheta, M., Taha, E.A., Lu, Y., and Eguchi, T. (2023). Extracellular Vesicles: New Classification and Tumor Immunosuppression. Preprint at MDPI, https://doi.org/10.3390/biology12010110 https://doi.org/10.3390/biology12010110.

9. Abels, E.R., and Breakefield, X.O. (2016). Introduction to Extracellular Vesicles: Biogenesis, RNA Cargo Selection, Content, Release, and Uptake. Preprint at Springer New York LLC, https://doi.org/10.1007/s10571-016-0366-z https://doi.org/10.1007/s10571-016-0366-z.

10. Yu, J., Sane, S., Kim, J.E., Yun, S., Kim, H.J., Jo, K.B., Wright, J.P., Khoshdoozmasouleh, N., Lee, K., Oh, H.T., et al. (2023). Biogenesis and delivery of extracellular vesicles: harnessing the power of EVs for diagnostics and therapeutics. Preprint at Frontiers

Media SA, https://doi.org/10.3389/fmolb.2023.1330400 https://doi.org/10.3389/fmolb.2023.1330400.

11. Welsh, J.A., Goberdhan, D.C.I., O'Driscoll, L., Buzas, E.I., Blenkiron, C., Bussolati, B., Cai, H., Di Vizio, D., Driedonks, T.A.P., Erdbrügger, U., et al. (2024). Minimal information for studies of extracellular vesicles (MISEV2023): From basic to advanced approaches. J. Extracell. Vesicles *13*. https://doi.org/10.1002/jev2.12404.

12. Petroni, D., Fabbri, C., Babboni, S., Menichetti, L., Basta, G., and Del Turco, S. (2023). Extracellular Vesicles and Intercellular Communication: Challenges for In Vivo Molecular Imaging and Tracking. Preprint at Multidisciplinary Digital Publishing Institute (MDPI), https://doi.org/10.3390/pharmaceutics15061639 https://doi.org/10.3390/pharmaceutics15061639.

13. Liu, Y.J., and Wang, C. (2023). A review of the regulatory mechanisms of extracellular vesicles-mediated intercellular communication. Preprint at BioMed Central Ltd, https://doi.org/10.1186/s12964-023-01103-6 https://doi.org/10.1186/s12964-023-01103-6.

14. Fang, F., Yang, J., Wang, J., Li, T., Wang, E., Zhang, D., Liu, X., and Zhou, C. (2024). The role and applications of extracellular vesicles in osteoporosis. Preprint at Springer Nature, https://doi.org/10.1038/s41413-023-00313-5 https://doi.org/10.1038/s41413-023-00313-5.

15. Pan, K., Zhu, Y., Chen, P., Yang, K., Chen, Y., Wang, Y., Dai, Z., Huang, Z., Zhong, P., Zhao, X., et al. (2024). Biological functions and biomedical applications of extracellular vesicles derived from blood cells. Preprint at Elsevier Inc., https://doi.org/10.1016/j.freeradbiomed.2024.06.002 https://doi.org/10.1016/j.freeradbiomed.2024.06.002.

16. Nieuwland, R., and Siljander, P.R.M. (2024). A beginner's guide to study extracellular vesicles in human blood plasma and serum. Preprint at John Wiley and Sons Inc, https://doi.org/10.1002/jev2.12400 https://doi.org/10.1002/jev2.12400.

17. Muttiah, B., Ng, S.L., Lokanathan, Y., Ng, M.H., and Law, J.X. (2024). Beyond Blood Clotting: The Many Roles of Platelet-Derived Extracellular Vesicles. Preprint at Multidisciplinary Digital Publishing Institute (MDPI), https://doi.org/10.3390/biomedicines12081850 https://doi.org/10.3390/biomedicines12081850.

18. Talbott, H.E., Mascharak, S., Griffin, M., Wan, D.C., and Longaker, M.T. (2022). Wound healing, fibroblast heterogeneity, and fibrosis. Preprint at Cell Press, https://doi.org/10.1016/j.stem.2022.07.006 https://doi.org/10.1016/j.stem.2022.07.006.

19. Plikus, M. V., Wang, X., Sinha, S., Forte, E., Thompson, S.M., Herzog, E.L., Driskell, R.R., Rosenthal, N., Biernaskie, J., and Horsley, V. (2021). Fibroblasts: Origins, definitions, and functions in health and disease. Preprint at Elsevier B.V., https://doi.org/10.1016/j.cell.2021.06.024 https://doi.org/10.1016/j.cell.2021.06.024.

20. Gauthier, V., Kyriazi, M., Nefla, M., Pucino, V., Raza, K., Buckley, C.D., and Alsaleh, G. (2023). Fibroblast heterogeneity: Keystone of tissue homeostasis and pathology in inflammation and ageing. Preprint at Frontiers Media S.A., https://doi.org/10.3389/fimmu.2023.1137659 https://doi.org/10.3389/fimmu.2023.1137659.

21. Almet, A.A., Liu, Y., Nie, Q., and Plikus, M. V. (2025). Integrated Single-Cell Analysis Reveals Spatially and Temporally Dynamic Heterogeneity in Fibroblast States during Wound Healing. Journal of Investigative Dermatology *145*, 645-659.e25. https://doi.org/10.1016/j.jid.2024.06.1281.

22. Lujano Olazaba, O., Farrow, J., and Monkkonen, T. (2024). Fibroblast heterogeneity and functions: insights from single-cell sequencing in wound healing, breast cancer, ovarian cancer and melanoma. Preprint at Frontiers Media SA, https://doi.org/10.3389/fgene.2024.1304853 https://doi.org/10.3389/fgene.2024.1304853.

23. Tracy, L.E., Minasian, R.A., and Caterson, E.J. (2016). Extracellular Matrix and Dermal Fibroblast Function in the Healing Wound. Preprint at Mary Ann Liebert Inc., https://doi.org/10.1089/wound.2014.0561 https://doi.org/10.1089/wound.2014.0561.

24. Cialdai, F., Risaliti, C., and Monici, M. (2022). Role of fibroblasts in wound healing and tissue remodeling on Earth and in space. Preprint at Frontiers Media S.A., https://doi.org/10.3389/fbioe.2022.958381 https://doi.org/10.3389/fbioe.2022.958381.

25. Mamun, A. Al, Shao, C., Geng, P., Wang, S., and Xiao, J. (2024). Recent advances in molecular mechanisms of skin wound healing and its treatments. Preprint at Frontiers Media SA, https://doi.org/10.3389/fimmu.2024.1395479 https://doi.org/10.3389/fimmu.2024.1395479.

26. Jin, C., Jin, Y., Ding, Z., Nuch, K.S., Han, M., Shim, J.H., Chien, P.N., and Heo, C.Y. (2025). Cellular and Molecular Mechanisms of Wound Repair: From Biology to Therapeutic Innovation. Preprint at Multidisciplinary Digital Publishing Institute (MDPI), https://doi.org/10.3390/cells14231850 https://doi.org/10.3390/cells14231850.

27. Singer, A.J. (2022). Healing Mechanisms in Cutaneous Wounds: Tipping the Balance. Preprint at Mary Ann Liebert Inc., https://doi.org/10.1089/ten.teb.2021.0114 https://doi.org/10.1089/ten.teb.2021.0114.

28. Rodrigues, M., Kosaric, N., Bonham, C.A., and Gurtner, G.C. (2019). Wound Healing: A Cellular Perspective. Physiol Rev *99*, 665–706. https://doi.org/10.1152/physrev.00067.2017.-Wound.

29. Olczyk, P., Mencner, Ł., and Komosinska-Vassev, K. (2014). The role of the extracellular matrix components in cutaneous wound healing. Preprint at Hindawi Publishing Corporation, https://doi.org/10.1155/2014/747584 https://doi.org/10.1155/2014/747584.

30. Fernández-Guarino, M., Hernández-Bule, M.L., and Bacci, S. (2023). Cellular and Molecular Processes in Wound Healing. Preprint at Multidisciplinary Digital Publishing

Institute (MDPI), https://doi.org/10.3390/biomedicines11092526 https://doi.org/10.3390/biomedicines11092526.

31. Peña, O.A., and Martin, P. (2024). Cellular and molecular mechanisms of skin wound healing. Preprint at Nature Research, https://doi.org/10.1038/s41580-024-00715-1 https://doi.org/10.1038/s41580-024-00715-1.

32. Diller, R.B., and Tabor, A.J. (2022). The Role of the Extracellular Matrix (ECM) in Wound Healing: A Review. Preprint at MDPI, https://doi.org/10.3390/biomimetics7030087 https://doi.org/10.3390/biomimetics7030087.

33. Gupta, A.K., Wang, T., Rapaport, J.A., and Talukder, M. (2025). Therapeutic Potential of Extracellular Vesicles (Exosomes) Derived From Platelet-Rich Plasma: A Literature Review. Preprint at John Wiley and Sons Inc, https://doi.org/10.1111/jocd.16709 https://doi.org/10.1111/jocd.16709.

34. Tao, S.C., Guo, S.C., and Zhang, C.Q. (2017). Platelet-derived extracellular vesicles: An emerging therapeutic approach. Preprint at Ivyspring International Publisher, https://doi.org/10.7150/ijbs.19776 https://doi.org/10.7150/ijbs.19776.